Journal of Alloys and Compounds 509 (2011) 5833–5838

Contents lists available at ScienceDirect

Journal of Alloys and Compounds

journal homepage: www.elsevier.com/locate/jallcom

Effects of oxygen content and heating rate on phase transition behavior in $Bi_2(V_{0.95}Ti_{0.05})O_{5.475-x}$

Yu-ki Taninouchi [a,*], Tetsuya Uda [b], Tetsu Ichitsubo [b], Yasuhiro Awakura [b], Eiichiro Matsubara [b]

[a] Department of Materials Science and Engineering, Kyoto University, Research Fellow of the Japan Society for the Promotion of Science, Kyoto 606-8501, Japan
[b] Department of Materials Science and Engineering, Kyoto University, Kyoto 606-8501, Japan

ARTICLE INFO

Article history:
Received 30 December 2010
Accepted 23 February 2011
Available online 3 March 2011

Keywords:
BIMEVOX
$Bi_2VO_{5.5}$
Phase transitions
Oxide-ion conductor
Doping

ABSTRACT

The phase transition behavior of oxide-ion conductor $Bi_2(V_{0.95}Ti_{0.05})O_{5.475-x}$, which has various thermal histories and sample forms, has been studied by means of differential scanning calorimetry. Thermogravimetric analysis revealed that the oxygen content per compositional formula varied with the applied thermal treatment, although no significant structural difference was observed by X-ray diffraction (XRD) analysis. The phase transition behavior from α_f to β_f and from β_f to γ_f, observed at a heating rate of 10 K min^{-1}, are markedly affected by the sample preparation. For example, the endothermic peak of the transition from α_f to β_f appeared at around 400 °C for quenched powder and at around 320 °C for powder cooled at 0.5 K min^{-1}. The trend of the transition temperatures can be qualitatively explained in terms of oxygen content, *i.e.*, $Bi_2(V_{0.95}Ti_{0.05})O_{5.475-x}$ with less oxygen content exhibits the transition from α_f to β_f at a higher temperature and the transition from β_f to γ_f at a lower temperature. We confirmed the two types of transition behavior from α_f to β_f depending on heating rate of DSC and high-temperature X-ray diffraction (HT-XRD) analysis. At rapid heating rates of 10 and 40 K min^{-1}, α_f transformed to β_f directly. Meanwhile, at a slow heating rate of 2 K min^{-1}, the β_f precipitated from α_f because slow heating allowed the diffusion of Ti and oxygen vacancies induced by the aliovalent doping. This suggests that the small differences of atomic arrangement also affect the phase transition behavior because additional elements have preferable crystallographic sites in α_f and β_f.

1. Introduction

Doped bismuth vanadate $Bi_2(V_{1-d}ME_d)O_{5.5+\delta}$ (ME: dopant metal, d: dopant concentration, δ: deviation of oxygen content due to aliovalent doping and/or partial reduction of pentavalent vanadium), so-called BIMEVOX [1–3], exhibits a characteristic phase transition behavior. It is a promising oxide-ion conductor at intermediate temperatures between 400 and 600 °C. The parent compound $Bi_2VO_{5.5}$ [4] and BIMEVOX itself have a single-layer Aurivillius structure and exhibit the three main polymorphs of monoclinic α, orthorhombic β, and tetragonal γ. The Aurivillius structure consists of alternating $(Bi_2O_2)^{2+}$ and $(V_{1-d}ME_dO_{3.5+\delta})^{2-}$ layers. These Bi–O and (V,ME)-O layers characterize the oxide-ion conduction in the present system. In the γ-phase shown in Fig. 1, the (V,ME)-O layer is made up of corner-sharing oxygen octahedrons containing oxygen vacancies (□), that is $(V_{1-d}ME_dO_{3.5+\delta}\square_{0.5-\delta})^{2-}$. The γ-phase containing disordered oxygen vacancies shows high oxide-ion conduction at high temperatures. The β- and α-phases are characterized by ordering of oxygen vacancies in the (V,ME)-O layer [5,6]. Besides the α-, β-, and γ-phases, several phases which deviate from the three main phases (*e.g.*, orthorhombic α-like-phase [7], tetragonal β-like-phase [8], ε-phase [9], γ′-phase [10,11]) are observed in $Bi_2VO_{5.5}$ and BIMEVOX. By focusing on the network structure in (V,ME)-O layer which controls the oxide-ion conduction, we have classified the complex polymorphs into three phase groups of γ_f (high-level disorder and high-conductive phases), β_f (intermediate-level disorder and intermediate-conductive phases), and α_f (high-level order and low-conductive phases) [12]. The strict crystalline symmetries are ignored in this phase classification. According to the practical phase classification system, $Bi_2VO_{5.5}$ exhibits the phase transition from α_f to β_f (α_f/β_f transition) and from β_f to γ_f (β_f/γ_f transition) at 445 and 570 °C, respectively. The oxide-ion conductivities of $Bi_2VO_{5.5}$ are more than 10^{-2} S cm^{-1} above 500 °C in β_f and about 5×10^{-1} S cm^{-1} at 700 °C in γ_f.

In $Bi_2(V_{0.95}TM_{0.05})O_{5.5+\delta}$ (TM = Ti, Zr, Hf, Nb, Ta, Mo, and W) [12], γ_f and/or β_f are stabilized at lower temperatures. Furthermore, the phase transition behavior of $Bi_2(V_{0.95}TM_{0.05})O_{5.5+\delta}$ varies with the thermal history although the samples have the same dopant composition. Among them, Ti-doped $Bi_2VO_{5.5}$ exhibited the highest stability against thermal decomposition and a strong effect of thermal history on electrical conductivity [12]. In the present

* Corresponding author. Tel.: +81 75 753 5456; fax: +81 75 753 5480.
E-mail address: taninouchi@mdsgn.mtl.kyoto-u.ac.jp (Y.-k. Taninouchi).

0925-8388/$ – see front matter © 2011 Elsevier B.V. All rights reserved.
doi:10.1016/j.jallcom.2011.02.137

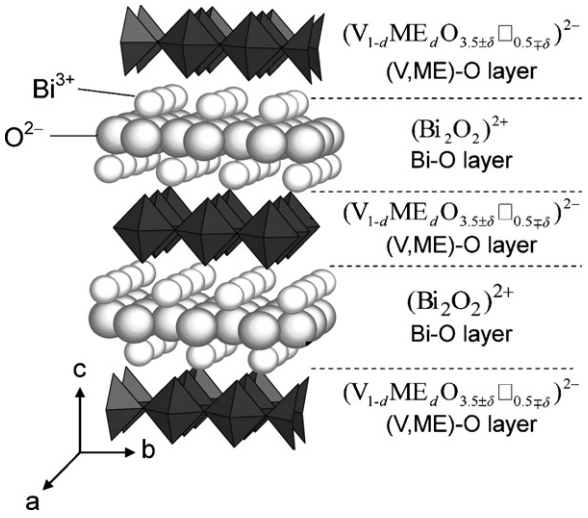

Fig. 1. Ideal structure of γ-phase of BIMEVOX. Oxygen vacancies exist in the (V,ME)-O layer consisting of V, doped ME, and O, although they are not shown.

Table 1
Abbreviations of $Bi_2(V_{0.95}Ti_{0.05})O_{5.475-x}$ with different sample forms and thermal treatments. $Bi_2(V_{0.95}Ti_{0.05})O_{5.475-x}$, where x refers to deviation induced by the partial reduction of transition metals, is denoted as Ti5. The powder and bulk samples are called as Ti5/P and Ti5/B, respectively. All samples were cooled in air from 800 °C, at which γ_f of Ti5 is stable.

Abbreviation	Sample form	Cooling rate in air from 800 °C
Ti5/P/CQ	Powder	Quench to room temperature
Ti5/P/C10		10 K min^{-1}
Ti5/P/C1		1 K min^{-1}
Ti5/P/C05		0.5 K min^{-1}
Ti5/B/CQ	Bulk	Quench to room temperature
Ti5/B/C10		10 K min^{-1}
Ti5/B/C1		1 K min^{-1}
Ti5/B/C05		0.5 K min^{-1}

study, careful investigations of the phase transition behavior of 5 mol% Ti-doped $Bi_2VO_{5.5}$ were studied by X-ray diffraction analyses, thermogravimetric analysis (TGA), and differential scanning calorimetry (DSC).

2. Experimental

5 mol% Ti-doped $Bi_2VO_{5.5}$, denoted as Ti5, was prepared in powder and bulk forms, as listed in Table 1. Because Ti exists in the tetravalent form in $Bi_2VO_{5.5}$, Ti5 can be formulated as $Bi_2(V_{0.95}Ti_{0.05})O_{5.475-x}$ (x: oxygen loss due to a partial reduction of the transition metals). We abbreviate the Ti5 powder sample as Ti5/P and the Ti5 bulk sample as Ti5/B. Fig. 2(a) shows a scanning electron microscope (SEM) image of the powder sample synthesized by a conventional solid-state reaction at 800 °C. Details of the synthesis process are given elsewhere [12]. The powder particle size was from 0.2 to 5 μm. Fig. 2(b) shows an optical microscope image of the surface of the bulk sample. A relative density of the bulk sample was 95%. The grains were well grown as large as 20 μm in size. The powder and bulk samples were cooled in air at various rates from 800 °C, at which γ_f of Ti5 is stable.

X-ray diffraction analyses at room temperature (XRD analysis) as well as high-temperature (HT-XRD analysis) were carried out using X'Pert PRO MPD (PANalytical, Cu-Kα radiation) and HTK-1200 N Oven Chamber (Anton Paar). HT-XRD profiles were collected for 10 min immediately after the samples were heated to the target temperatures.

Thermogravimetric analysis (TGA) was performed using a DTG-60H (Shimadzu) in order to evaluate the variation of oxygen content with temperature. Powder samples of ~320 mg in platinum containers were kept at 150 °C for 2 h for drying and then heated at 5 K min^{-1} to 800 °C in flowing air. To calculate the oxygen content per compositional formula, we assume that weight changes could be attributed only to the uptake and loss of oxygen, which is caused by the partial reduction or oxidation of the transition metals. The slowly cooled powder of Ti5/P/C05 were considered to be fully oxidized ($x = 0$), *i.e.*, the composition of as-prepared Ti5/P/C05 was $Bi_2(V_{0.95}Ti_{0.05})O_{5.475}$. To evaluate the oxygen contents of the quenched powder Ti5/P/CQ, we assumed that Ti5/P/CQ after re-heating to 800 °C has the same oxygen content with Ti5/P/C05 at 800 °C.

DSC was carried out using a Diamond differential scanning calorimeter (PerkinElmer) with a platinum container. The samples were heated in stagnant air at 2, 5, 10, or 40 K min^{-1}. The onset temperature of each endothermic peak was evaluated by the intersection point method with an error of ±2 °C.

3. Results

3.1. XRD profiles of powders cooled at various rates

Fig. 3(a) shows the XRD patterns of Ti5/P cooled at various rates. The calculated pattern of monoclinic α-$Bi_2VO_{5.5}$ at Cu-Kα_1 radiation [6] is also given as a reference pattern of α_f. The structures of the three phase groups are characterized by an orthorhombic subcell of $a_m = 0.55$, $b_m = 0.56$, and $c_m = 1.53$ nm, *i.e.*, $a \approx 3a_m$, $b \approx b_m$, $c \approx c_m$ for α_f, $a \approx 2a_m$, $b \approx b_m$, $c \approx c_m$ for β_f, and $a \approx a_m$, $b \approx b_m$, $c \approx c_m$ for γ_f. The diffraction peaks are indexed based on the orthorhombic subcell of a_m, b_m and c_m. Ideal α_f-$Bi_2VO_{5.5}$ exhibits superlattice diffractions, such as 1/3 1 3 at ~24.2°, and has monoclinic symmetry, as verified by the splitting of 2 2 0 at ~46°. Meanwhile, orthorhombic α_f was stabilized in Ti5/P/CQ, C10, C1, and C05, as shown in Fig. 3(a). There was little change in the lattice constants of a_m, b_m, and c_m with the cooling rate, as shown in Fig. 3(b).

3.2. Temperature dependence of oxygen content

Fig. 4 shows the oxygen content of Ti5/P/CQ and Ti5/P/C05 as a function of temperature. Partial reduction proceeded in the fully-oxidized sample of Ti5/P/C05 above ~540 °C. The onset temperature of the partial reduction is immediately above the temperature of the β_f/γ_f transition determined by DSC. The oxygen content decreased to 5.469 ± 0.002 ($x = 0.006 \pm 0.002$) at 800 °C. Meanwhile, the quenched powder Ti5/P/CQ exhibited the oxygen uptake from 300 to 500 °C, and oxygen loss above ~540 °C. The oxygen content of Ti5/P/CQ at 200 °C was evaluated as 5.470 ± 0.002 ($x = 0.005 \pm 0.002$). Assuming that the vanadium was partially reduced from V^{+5} to V^{+4}, the composition of as-prepared

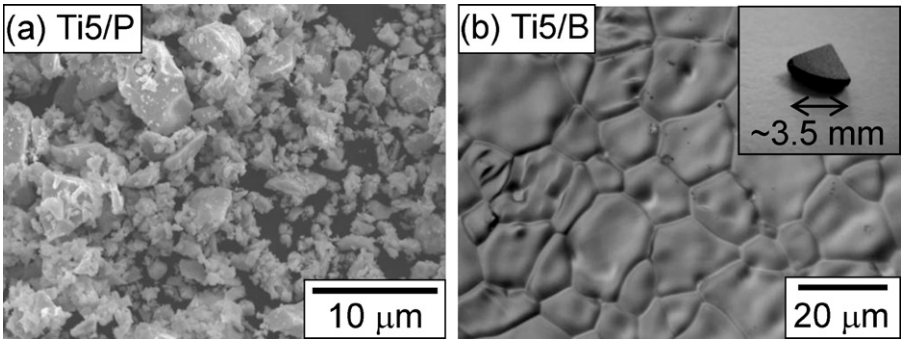

Fig. 2. (a) SEM image of powder sample, Ti5/P. (b) Optical microscope image of surface of bulk sample, Ti5/B. An image of the entire bulk sample is shown in the inset.

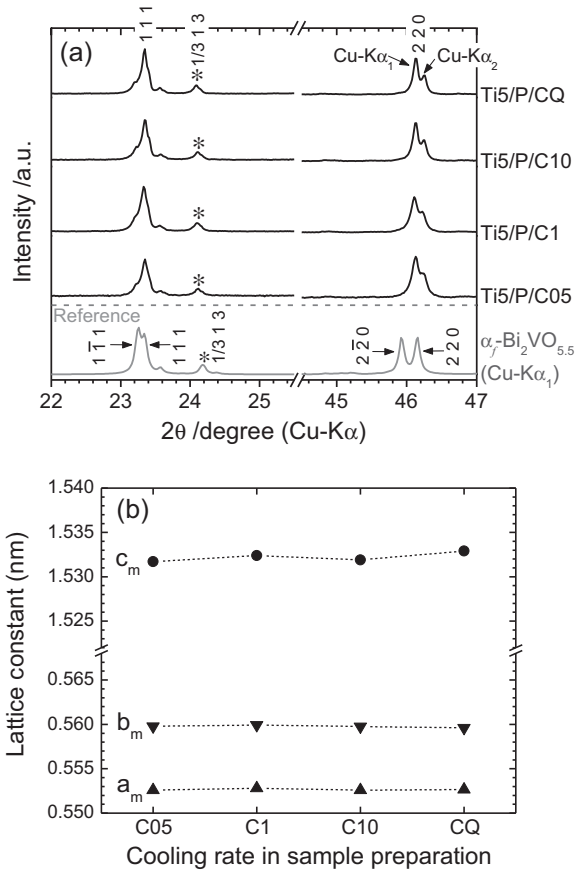

Fig. 3. (a) XRD patterns of Ti5/P cooled at various rates. The pattern of monoclinic α_f-$Bi_2VO_{5.5}$ calculated at Cu-Kα_1 radiation is also shown as a reference. Plane indices are marked assuming a mean orthorhombic subcell. Asterisks (*) indicate typical superlattice diffractions of α_f, *i.e.*, 1/3 1 3 peak. (b) Lattice constants of the subcell.

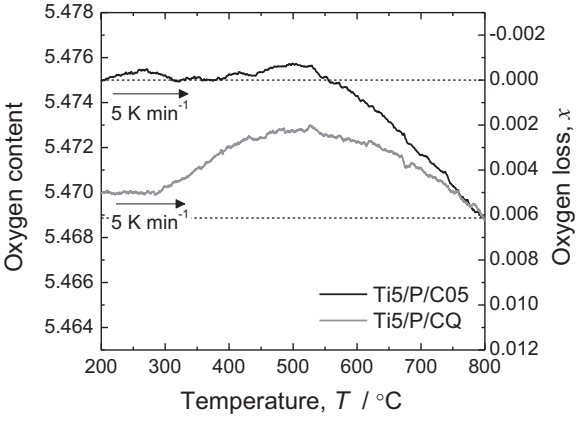

Fig. 4. Temperature dependence of oxygen content of Ti5/P/C05 and Ti5/P/CQ. TGA was performed in air at a heating rate of 5 K min^{-1}. The oxygen content of as-prepared Ti5/P/C05 was regarded to be the fully oxidized value of 5.475. We assumed that at 800 °C the oxygen content of Ti5/P/CQ coincided with that of Ti5/P/C05.

Ti5/P/CQ can be described as $Bi_2(V^{+5}_{0.94}V^{+4}_{0.01}Ti^{+4}_{0.05})O_{5.470}$. The difference in oxygen content between Ti5/P/C05 and Ti5/P/CQ gradually decreased above 300 °C.

3.3. Variation in DSC profiles induced by the sample preparation

Fig. 5 shows the DSC profiles of the powder and bulk samples cooled in air at various rates. All profiles were collected at the same

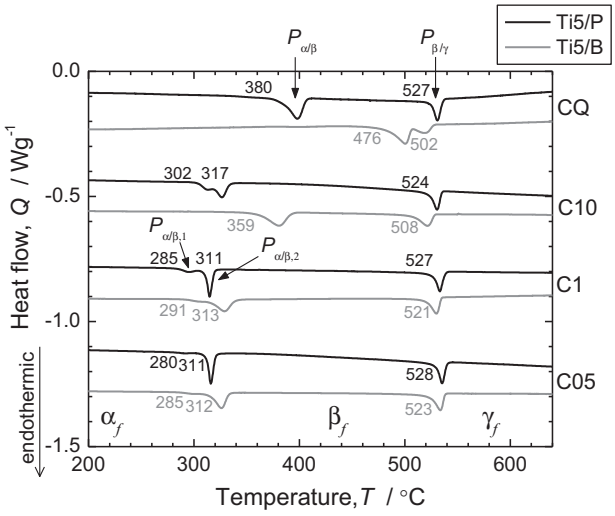

Fig. 5. DSC profiles of Ti5/P and Ti5/B cooled in air at various rates. All profiles were collected in air at a heating rate of 10 K min^{-1}. Numerical values are onset temperatures of endothermic peaks. $P_{\alpha/\beta}$ and $P_{\beta/\gamma}$ refer to endothermic peaks corresponding to α_f/β_f and β_f/γ_f transitions, respectively. Slowly cooled samples exhibited the splitting of $P_{\alpha/\beta}$ into $P_{\alpha/\beta,1}$ and $P_{\alpha/\beta,2}$.

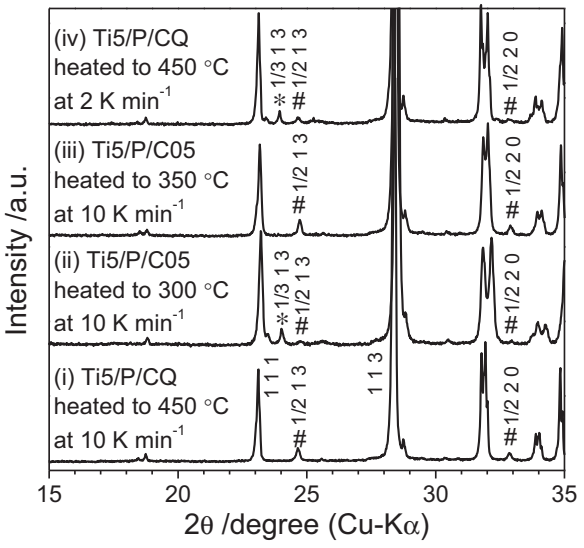

Fig. 6. HT-XRD patterns of (i) Ti5/P/CQ heated to 450 °C at 10 K min^{-1}, (ii) Ti5/P/C05 heated to 300 °C at 10 K min^{-1}, (iii) Ti5/P/C05 heated to 350 °C at 10 K min^{-1}, and (iv) Ti5/P/CQ heated to 450 °C at 2 K min^{-1}. Plane indices are marked assuming a mean orthorhombic subcell. Asterisks (*) and hashes (#) indicate typical superlattice diffractions of α_f and β_f, respectively.

heating rate of 10 K min^{-1}. First, we focus our attention on the profiles of the powder samples, *i.e.*, the darker profiles. In the DSC profiles of Ti5/P/CQ, two endothermic peaks appeared at around 400 and 530 °C. When Ti5/P/CQ was heated to 450 °C at 10 K min^{-1} in another experiment, β_f was obtained, as indicated by the HT-XRD pattern (i) in Fig. 6. Thus, the endothermic peak at around 400 °C corresponds to the α_f/β_f transition, and that at around 530 °C corresponds to the β_f/γ_f transition. We call the endothermic peak for the α_f/β_f transition $P_{\alpha/\beta}$ and that for the β_f/γ_f transition $P_{\beta/\gamma}$. In addition, the onset temperatures of the α_f/β_f and β_f/γ_f transitions are termed $T_{\alpha/\beta}$ and $T_{\beta/\gamma}$, respectively.

The DSC profiles of Ti5/P varied markedly with the cooling rate. $P_{\alpha/\beta}$ shifted from 400 to 320 °C with a decrease in the cooling rate, although $P_{\beta/\gamma}$ remained unchanged. In the DSC profiles of Ti5/P/C10, C1, and C05, $P_{\alpha/\beta}$ split into two peaks, *i.e.*, a smaller

peak at a lower temperature, $P_{\alpha/\beta,1}$, and a larger peak at a higher temperature, $P_{\alpha/\beta,2}$. $P_{\alpha/\beta,1}$ decreased with the cooling rate. The onset temperatures of $P_{\alpha/\beta,1}$ and $P_{\alpha/\beta,2}$ are denoted $T_{\alpha/\beta,1}$ and $T_{\alpha/\beta,2}$, respectively. HT-XRD patterns of Ti5/P/C05 heated to 300 and 350 °C at 10 K min^{-1} are shown as patterns (ii) and (iii) in Fig. 6. At 300 °C between $T_{\alpha/\beta,1}$ and $T_{\alpha/\beta,2}$, the main phase was α_f, and a small amount of β_f also existed. Meanwhile, the single phase of β_f was obtained at 350 °C above $T_{\alpha/\beta,2}$. This indicates that the two different types of α_f existed in as-prepared Ti5/P/C05 and exhibited transitions at $T_{\alpha/\beta,1}$ and $T_{\alpha/\beta,2}$. For non-doped $Bi_2VO_{5.5}$, such a wide variation of the DSC profiles was not seen when same measurements were performed for powder samples cooled at various rates (data are not shown).

The DSC profiles of the bulk samples are shown as gray profiles in Fig. 5. Phase transition behavior of Ti5/B was markedly affected by the cooling rate. In the DSC profile of Ti5/B/CQ, $P_{\alpha/\beta}$ appeared at around 500 °C and the temperature region of β_f was narrow. $P_{\alpha/\beta}$ for Ti5/B/C1 and C05 was split into $P_{\alpha/\beta,1}$ and $P_{\alpha/\beta,2}$ because slow cooling caused a formation of slight amount of the polymorphs of α_f. For Ti5/B, $P_{\alpha/\beta}$ shifted to a lower temperature with a decrease in the cooling rate. This trend agrees with that observed for Ti5/P. However, $T_{\beta/\gamma}$ for Ti5/B increased with a decrease in the cooling rate. Comparing the DSC profile of Ti5/B to that of Ti5/P at a given cooling rate indicated that $P_{\alpha/\beta}$ for Ti5/B appeared at a higher temperature than that for Ti5/P. $T_{\beta/\gamma}$ for Ti5/B was lower than that for Ti5/P at a given cooling rate. The difference between the transition behaviors of Ti5/B and Ti5/P became small in slowly cooled samples.

3.4. Variation in DSC profiles induced by the DSC heating rate

Fig. 7(a) shows the DSC profiles of Ti5/P/CQ collected at heating rates of 2, 5, 10, and 40 K min^{-1}. At the slower heating rates of 5 and 2 K min^{-1}, $P_{\alpha/\beta}$ apparently split into two broad peaks, *i.e.*, a large endothermic peak appeared at around 500 °C in addition to the endothermic peak at around 400 °C. Endothermic reaction occurred successively between two endothermic peaks at the heating rates below 5 K min^{-1}. For the split $P_{\alpha/\beta}$, we term the endothermic peaks at lower and higher temperatures $P_{\alpha/\beta,L}$ and $P_{\alpha/\beta,H}$, respectively. The onset temperatures of $P_{\alpha/\beta,L}$ and $P_{\alpha/\beta,H}$ are defined as $T_{\alpha/\beta,L}$ and $T_{\alpha/\beta,H}$, respectively. The HT-XRD pattern of Ti5/P/CQ heated to 450 °C at 10 and 2 K min^{-1} is shown in Fig. 6 as patterns (i) and (iv), respectively. Only β_f was obtained at a heating rate of 10 K min^{-1}. When Ti5/P/CQ was heated at 2 K min^{-1}, however, a mixture of α_f and β_f was obtained at 450 °C which is an intermediate temperature between $T_{\alpha/\beta,L}$ and $T_{\alpha/\beta,H}$.

Fig. 7(b) shows the DSC profiles of Ti5/P/C05 at the various heating rates. $P_{\alpha/\beta,1}$ and $P_{\alpha/\beta,2}$ appeared in the DSC profiles at the higher heating rates of 5, 10, and 40 K min^{-1}, because as-prepared Ti5/P/C05 contained a small amount of polymorphic α_f. $T_{\alpha/\beta,1}$ and $T_{\alpha/\beta,2}$ did not change with heating rate for 5, 10, and 40 K min^{-1}. The DSC profile at the slower heating rate of 2 K min^{-1} was very different. The trace of $P_{\alpha/\beta,1}$ existed at around 290 °C. The larger endothermic peak $P_{\alpha/\beta,2}$, however, apparently split into two broad peaks $P_{\alpha/\beta,L}$ and $P_{\alpha/\beta,H}$, which appeared from 318 to 403 °C.

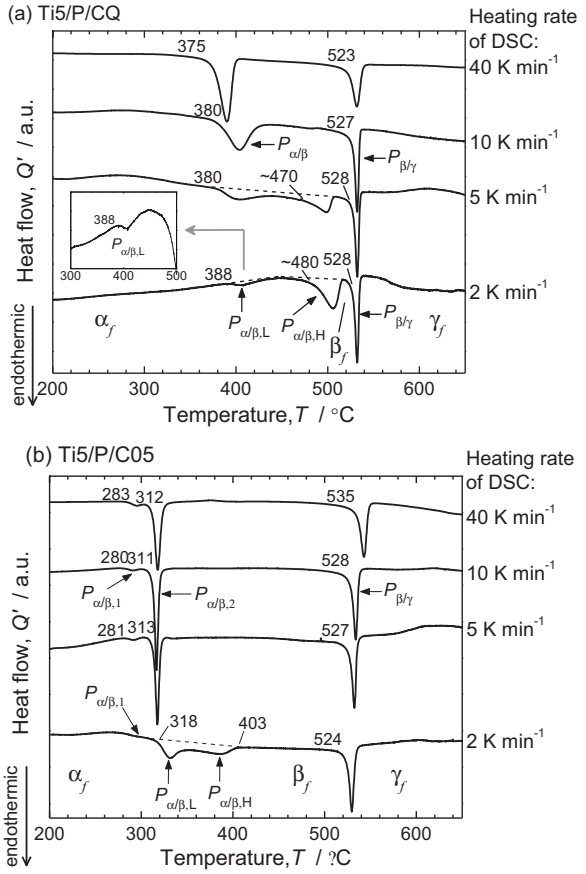

Fig. 7. DSC profiles of (a) Ti5/P/CQ and (b) Ti5/P/C05 collected in air at heating rates of 2, 5, 10, and 40 K min^{-1}. The represented heat flow is the value divided by the heating rate. At slow heating rates, $T_{\alpha/\beta}$ for Ti5/P/CQ and $T_{\alpha/\beta,2}$ for Ti5/P/C05 exhibited splitting into $P_{\alpha/\beta,L}$ and $P_{\alpha/\beta,H}$.

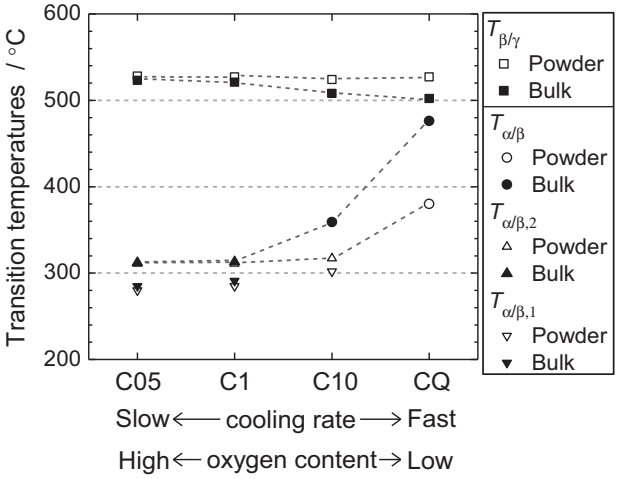

Fig. 8. Variation of transition temperatures evaluated by DSC at a heating rate of 10 K min^{-1}. $T_{\alpha/\beta}$, $T_{\alpha/\beta,1}$, $T_{\alpha/\beta,2}$, and $T_{\beta/\gamma}$ determined in Fig. 5 are plotted. Samples cooled at faster rates should have less oxygen content before analysis. When cooled at the same rate, the bulk sample should have less oxygen content than the powder sample.

4. Discussion

4.1. Variation in phase transition temperatures induced by the sample preparation

The difference in the sample preparation drastically changed the phase transition behavior of Ti5. The variation of transition temperatures can be qualitatively explained in terms of the oxygen content in the samples. Fig. 8 summarizes the transition temperatures evaluated by the DSC profiles at a heating rate of 10 K min^{-1} in Fig. 5. As verified by TGA in Fig. 4, the quenched samples has the less oxygen content. This is because Ti5 exhibited partial reduction at 800 °C and the oxygen supply during the cooling process is not enough. That is, samples cooled at faster rates should have less oxygen content than the thermally equilibrated value. Even if cooled at the same rate,

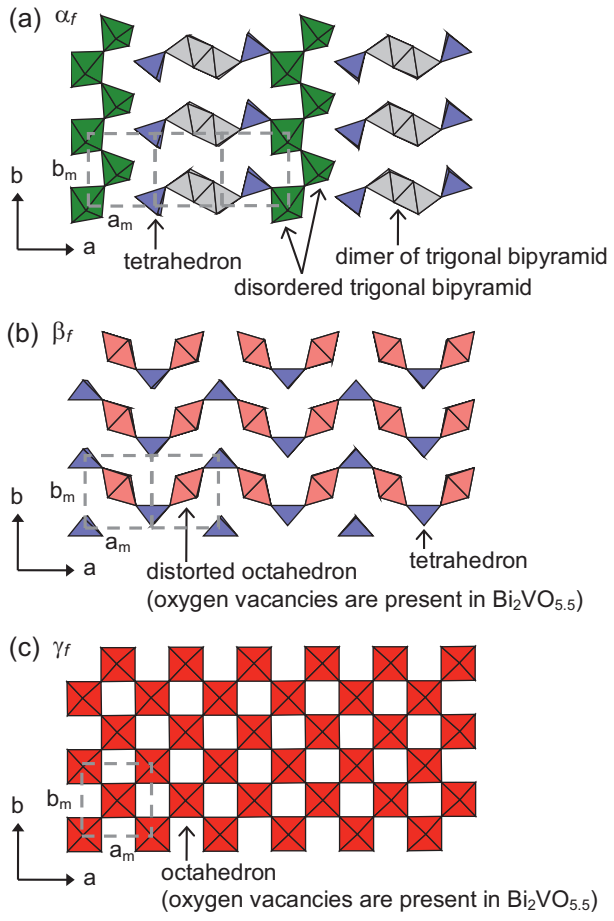

Fig. 9. Oxygen polyhedron network structures in the (V,ME)-O layers of (a) α_f, (b) β_f, and (c) γ_f. The network structures were schematically described based on the crystalline data of α-, β-, and γ-$Bi_2VO_{5.5}$ reported by Mairesse et al. [5,6]. Vanadium and dopants locate inside of oxygen polyhedron. Gray boxes represent the subcells to characterize each phase, *i.e.*, $a \approx 3a_m$, $b \approx b_m$, $c \approx c_m$ for α_f, $a \approx 2a_m$, $b \approx b_m$, $c \approx c_m$ for β_f, and $a \approx a_m$, $b \approx b_m$, $c \approx c_m$ for γ_f. In Ti5, doped Ti should exist in vanadium sites, and aliovalent doping should cause the oxygen vacancies for oxygen sites to preserve the electroneutrality.

the bulk sample should have less oxygen content than the powder sample due to the lower specific surface area of bulk sample, which requires longer-range diffusion of oxygen. According to Fig. 8, we noted the two experimental facts, *i.e.*, (i) Ti5 with less oxygen content exhibits the α_f/β_f transition at a higher temperature, and (ii) Ti5 with less oxygen content exhibits the β_f/γ_f transition at a lower temperature, although the latter trend is seen only in the bulk sample. The TGA profile of Ti5/P/CQ in Fig. 4 indicates that the oxidation gradually proceeds above 300 °C in the partially reduced sample. The oxygen supply in bulk sample on the DSC heating is expected to be much slower. As a results, in the bulk sample, the oxygen content is maintained to be lower than the thermodynamically equilibrated value even at a higher-temperature of β_f/γ_f transition, which leads to the variation in $T_{\beta/\gamma}$.

From the crystalline structure of $Bi_2VO_{5.5}$ reported by Mairesse et al. [5,6], the network structure of oxygen polyhedra in the (V/ME)-O layer differs among α_f, β_f, and γ_f, as shown in Fig. 9. Furthermore, vanadium takes multiple crystallographic positions in α_f and β_f, but its crystallographic position is unique in γ_f. It is, therefore, possible that Ti and oxygen vacancies induced by aliovalent doping take preferential sites in thermally equilibrated α_f and β_f. All the Ti5 samples were cooled from γ_f to α_f at finite rates. Thus, a small difference probably exists in the atomic arrangement of the (V/ME)-O layer. We consider that this structural difference also affects the variation in phase transition behavior, although it was quite difficult to identify it by our XRD analysis.

4.2. Effect of DSC heating rate on phase transition behavior

Slow DSC heating rates caused a peak split and continuous endothermic reaction of $P_{\alpha/\beta}$ for Ti5/P/CQ and C05, as shown in Fig. 7. The difference in oxygen content cannot account for this behavior because Ti5/P/C05 did not exhibit the uptake and loss of oxygen below 540 °C. We can explain the splitting and continuous endothermic reaction of $P_{\alpha/\beta}$ by a precipitation of β_f due to the progression of rearrangement of Ti and oxygen vacancies induced by aliovalent doping during slow heating.

HT-XRD patterns (i) and (iv) in Fig. 6 verify that, after Ti5/P/CQ was heated to 450 °C, only β_f was obtained at a heating rate of 10 K min^{-1}, but a mixture of α_f and β_f was obtained at a heating rate of 2 K min^{-1}. In the DSC profile of Ti5/P/CQ shown in Fig. 7(a), 450 °C was above the temperature range of $P_{\alpha/\beta}$ at a heating rate of 10 K min^{-1}, but was between the temperature range of $P_{\alpha/\beta,L}$ and $P_{\alpha/\beta,H}$ at a heating rate of 2 K min^{-1}. This means that, at a sufficiently slow heating rates, β_f can start precipitating from α_f at $T_{\alpha/\beta,L}$ and a mixture of α_f and β_f is observed in the temperature region of $P_{\alpha/\beta,L}$ and $P_{\alpha/\beta,H}$. The diffusion of Ti and oxygen vacancies induced by doping sufficiently occurs when α_f of Ti5 is heated at sufficiently slow rates. We believe that such atomic rearrangement during slow heating enhances the structural and/or compositional inhomogeneity in α_f and causes the splitting and continuous endothermic reaction of $P_{\alpha/\beta}$. This discussion further indicates that Ti and oxygen vacancies induced by doping probably have the preferential crystallographic sites in the (V/ME)-O layer shown in Fig. 9. Our findings indicate that the small differences of not only oxygen content but also the positions of dopant and oxygen vacancies are important to understand the wide variation in the polymorphic of Ti5. This might apply to other BIMEVOX compounds and help us understands their polymorphism. Further research on the local structures of dopant and oxygen vacancies in (V/ME)-O layer would clarify our idea.

5. Conclusion

We have determined the phase transition behavior of high oxide-ion conductor $Bi_2(V_{0.95}Ti_{0.05})O_{5.475-x}$ (x: oxygen loss due to a partial reduction). The phase transition behavior from α_f to β_f and from β_f to γ_f varies markedly with sample preparation as well as heating rate. Our findings are summarized as follows:

(1) The variation in transition temperatures at the same heating rate of 10 K min^{-1} is qualitatively explained in terms of oxygen content per chemical formula, which depends on thermal history and physical form of sample. We obtained empirical knowledge: $Bi_2(V_{0.95}Ti_{0.05})O_{5.475-x}$ with less oxygen content exhibits transition from α_f to β_f at a higher temperature and the transition from β_f to γ_f at a lower temperature. In particular, the transition temperature from α_f to β_f shows large variation; powder sample cooled at 0.5 K min^{-1} from 800 °C, whose oxygen content was 5.475, transformed to β_f at 311 °C. Meanwhile, powder sample quenched from 800 °C, whose oxygen content was 5.470 ± 0.002, transformed to β_f at 380 °C.
(2) Two types of phase transition behavior from α_f to β_f are observed depending on the heating rate. α_f directly transformed to β_f at fast rates of 10 and 40 K min^{-1}. Meanwhile, at a slower heating rate of 2 K min^{-1}, β_f precipitated from α_f due to the sufficient diffusion of Ti and oxygen vacancies induced by the aliovalent doping, and the co-existence of α_f and β_f was confirmed by HT-XRD analysis.

Acknowledgment

This work was financially supported by a Grant-in-Aid for JSPS fellows.

References

[1] F. Abraham, J.C. Boivin, G. Mairesse, G. Nowogrocki, Solid State Ionics 40–41 (1990) 934.
[2] J.C. Boivin, G. Mairesse, Chem. Mater. 10 (1998) 2870.
[3] G. Mairesse, C.R. Acad, Sci. Paris, Ser. IIc 2 (1999) 651.
[4] F. Abraham, M.F. Debreuille-Gresse, G. Mairesse, G. Nowogrocki, Solid State Ionics 28–30 (1988) 529.
[5] G. Mairesse, P. Roussel, R.N. Vannier, M. Anne, C. Pirovano, G. Nowogrocki, Solid State Sci. 5 (2003) 851.
[6] G. Mairesse, P. Roussel, R.N. Vannier, M. Anne, G. Nowogrocki, Solid State Sci. 5 (2003) 861.
[7] Y. Taninouchi, T. Uda, T. Ichitsubo, Y. Awakura, E. Matsubara, Mater. Trans. 51 (3) (2010) 561.
[8] M. Huve, R.N. Vannier, G. Nowogrocki, G. Mairesse, G.V. Tendeloo, J. Mater. Chem. 6 (8) (1996) 1339.
[9] I. Abrahams, F. Krok, M. Malys, W. Wrobel, Solid State Ionics 176 (2005) 2053.
[10] E. Pernot, M. Anne, M. Bacmann, P. Strobel, J. Fouletier, R.N. Vannier, G. Mairesse, F. Abraham, G. Nowogrocki, Solid State Ionics 70–71 (1994) 259.
[11] A. Watanabe, K. Das, J. Solid State Chem. 163 (2002) 224.
[12] Y. Taninouchi, T. Uda, T. Ichitsubo, Y. Awakura, E. Matsubara, Solid State Ionics 181 (2010) 1279.